Acta Crystallographica Section F
Structural Biology and Crystallization Communications
ISSN 1744-3091

Crystallization and preliminary X-ray diffraction analysis of selenophosphate synthetases from *Trypanosoma brucei* and *Leishmania major*

Lívia Maria Faim,[a] Ivan Rosa e Silva,[a] Marcio Vinicius Bertacine Dias,[b,c] Humberto D'Muniz Pereira,[a] José Brandao-Neto,[d] Marco Túlio Alves da Silva[a] and Otavio Henrique Thiemann[a]*

[a]Institute of Physics, University of São Paulo, Avenida Trabalhador São-carlense 400, 13566-590 São Carlos-SP, Brazil, [b]Department of Biochemistry, University of Cambridge, 80 Tennis Court Road, Cambridge CB2 1GA, England, [c]Brazilian Biosciences National Laboratory (LNBio), Brazilian Center of Research in Energy and Materials (CNPEM), Caixa Postal 6192, 13083-970 Campinas-SP, Brazil, and [d]Diamond Light Source, Harwell Science and Innovation Campus, Didcot OX11 0DE, England

Correspondence e-mail: thiemann@ifsc.usp.br

Received 5 March 2013
Accepted 27 May 2013

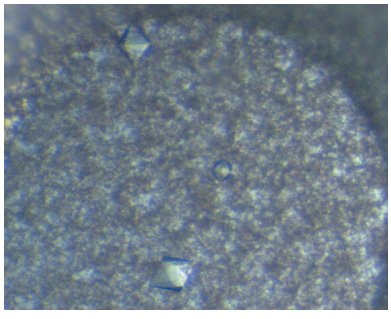

Selenophosphate synthetase (SPS) plays an indispensable role in selenium metabolism, being responsible for catalyzing the activation of selenide with adenosine 5′-triphosphate (ATP) to generate selenophosphate, the essential selenium donor for selenocysteine synthesis. Recombinant full-length *Leishmania major* SPS (*Lm*SPS2) was recalcitrant to crystallization. Therefore, a limited proteolysis technique was used and a stable N-terminal truncated construct (ΔN-*Lm*SPS2) yielded suitable crystals. The *Trypanosoma brucei* SPS orthologue (*Tb*SPS2) was crystallized by the microbatch method using paraffin oil. X-ray diffraction data were collected to resolutions of 1.9 Å for ΔN-*Lm*SPS2 and 3.4 Å for *Tb*SPS2.

1. Introduction

Selenophosphate synthetase (SPS; EC 2.7.9.3) is a central enzyme in selenocysteine (Sec) biosynthesis (Leinfelder *et al.*, 1990; Donovan & Copeland, 2010), catalyzing the production of monoselenophosphate (SeP). The reaction occurs by the activation of selenide with ATP and water, in a 1:1:1 stoichiometry, resulting in the formation of adenosine 5′-monophosphate (AMP), orthophosphate (P_i) and the biologically active form of selenium, monoselenophosphate (SeP) (Glass *et al.*, 1993; Veres *et al.*, 1994; Noinaj *et al.*, 2012).

Recent reports have demonstrated that SeP is derived from the transfer of the γ-phosphate group of ATP to selenide, while the β-phosphate group is released as orthophosphate (Itoh *et al.*, 2009; Wang *et al.*, 2009; Noinaj *et al.*, 2012).

SPSs are found in all domains of life (Su *et al.*, 2009) and have a conserved cysteine or selenocysteine residue in the N-terminal glycine-rich region corresponding to the catalytic site (Persson *et al.*, 1997; Sculaccio *et al.*, 2008). The kinetoplastid SPSs from *Trypanosoma brucei* (*Tb*SPS2) and *Leishmania major* (*Lm*SPS2), which share 26 and 28% amino-acid sequence identity with the *Escherichia coli* orthologue, respectively, are not selenoproteins (Sculaccio *et al.*, 2008), in contrast to the mammalian SPS2 selenoprotein. Initially considered to be irrelevant for *T. brucei* metabolism (Aeby *et al.*, 2009), *Tb*SPS2 is indeed involved in oxidative stress protection. In this organism, *Sps2* silencing reduced cell viability under hydrogen peroxide treatment or excessive growth, establishing its importance in cellular metabolism (Costa *et al.*, 2011).

Crystal structures have been reported of *Aquifex aeolicus* SPS (*Aa*SPS; 27 and 29% amino-acid sequence identity to *Tb*SPS2 and *Lm*SPS2, respectively) in the apo form and in complex with the nonhydrolyzable AMPCPP (α,β-methyleneadenosine 5′-triphosphate) (Matsumoto *et al.*, 2008; Itoh *et al.*, 2009). For human SPS1 (*Hs*SPS1; 42% amino-acid sequence identity to both *Tb*SPS2 and *Lm*SPS2), structures of complexes with AMPCPP, ADP and P_i products have been reported (Wang *et al.*, 2009). Recently, the structure of the *E. coli* SPS (*Ec*SPS) C17S mutant (the mutation site corresponds to positions Cys42 and Cys46 in *Tb*SPS2 and *Lm*SPS2, respectively) was solved in the apo form (Noinaj *et al.*, 2012). In these structures, metal ions such as Na^+ and K^+ were demonstrated to mediate the binding of the highly electronegative substrate phosphate group. In *Aa*SPS structures, both open and closed forms of the N-terminal Gly-rich loop have been observed and there is evidence

Table 1
Data-collection statistics for ΔN-*Lm*SPS2 and *Tb*SPS2.

Values in parentheses are for the outermost resolution shell.

	ΔN-*Lm*SPS2	*Tb*SPS2
Data-collection parameters		
X-ray source	DLS beamline I04-1	DLS beamline I04-1
Wavelength (Å)	0.92	0.92
Detector	PILATUS 2M	PILATUS 2M
Crystal-to-detector distance (mm)	237.0	325.2
Oscillation range per image (°)	0.25	0.35
No. of images	600	400
Crystal parameters		
Space group	$I2_12_12_1$	$P6_422$
No of molecules in asymmetric unit	1	1
Unit-cell parameters (Å)	a = 55.95, b = 81.69, c = 177.92	$a = b$ = 110.69, c = 142.93
Solvent content (%)	57.21	58.18
V_M (Å^3 Da^{-1})	2.87	2.94
Resolution range (Å)	40.97–1.88 (1.98–1.88)	57.29–3.40 (3.60–3.40)
$R_{p.i.m.}$† (%)	3.8 (39.3)	2.2 (15.0)
$\langle I/\sigma(I)\rangle$	11.4 (2.8)	20.7 (4.8)
Total No. of observations	167436 (24993)	134256 (10398)
No. of unique reflections	33416 (4849)	9061 (1285)
Multiplicity	5.0 (5.2)	13.1 (14.3)
Completeness (%)	97.7 (99.9)	99.9 (100.0)

† $R_{p.i.m.} = \sum_{hkl}\{1/[N(hkl)-1]\}^{1/2}\sum_i |I_i(hkl) - \langle I(hkl)\rangle|/\sum_{hkl}\sum_i I_i(hkl)$, where $I_i(hkl)$ is the intensity of observation i of reflection hkl and $N(hkl)$ is the redundancy of reflection hkl (Weiss & Hilgenfeld, 1997; Weiss *et al.*, 1998; Weiss, 2001).

that ATP binding, metal binding and the formation of their binding sites are interdependent (Itoh *et al.*, 2009). *Aa*SPS and *Hs*SPS1 are selective for monovalent cations, with a preference for K^+ over Na^+ or Li^+ (Wang *et al.*, 2009).

Here, we report the first crystallization and preliminary X-ray diffraction analysis of SPS2 from the kinetoplastid parasites *L. major* and *T. brucei*, which are not selenoproteins. Our structures may provide new information on the reaction mechanism of these enzymes. Moreover, comparison of the *Tb*SPS2 and *Lm*SPS2 structures with those of *Aa*SPS, *Hs*SPS1 and *Ec*SPS may contribute to an understanding of the evolution of the selenocysteine-biosynthesis pathway.

2. Materials and methods

2.1. Overexpression and purification of *Lm*SPS2 and *Tb*SPS2

*Lm*SPS2 (UniProt code Q4Q0M0) and *Tb*SPS2 (UniProt code Q38A34) cloned into pET28a were transformed in *E. coli* BL21 (DE3) cells, expressed and purified by adapting a previously described protocol (Sculaccio *et al.*, 2008). Briefly, cells were grown in LB medium containing 50 µg ml^{-1} kanamycin with agitation at 310 K until the OD at 600 nm of the cell culture reached 0.5–0.6. Protein expression was induced by the addition of isopropyl β-D-1-thio-galactopyranoside (IPTG) to a final concentration of 1.0 m*M* for 16 h under the same conditions. The cells were harvested by centrifugation at 4000*g* for 40 min and the cell pellet was suspended in 50 ml lysis buffer [50 m*M* Tris–HCl pH 8.0, 300 m*M* NaCl, 5%(*v*/*v*) glycerol, 1 m*M* β-mercaptoethanol and one tablet of Complete Protease Inhibitor Cocktail (Roche)]. The cells were disrupted by six cycles of 30 s sonication at 35 W (550 Sonic Dismembrator) and 30 s resting on ice.

The cell lysate was clarified by centrifugation at 20 000*g* for 30 min (277 K) and the cleared supernatant was applied onto a 5 ml Ni Sepharose High Performance HisTrap HP column (GE Healthcare) pre-equilibrated with buffer *A* (50 m*M* Tris–HCl pH 8.0, 300 m*M* NaCl, 1 m*M* β-mercaptoethanol, 10 m*M* imidazole). The column was washed with ten column volumes of buffer *A* and the bound protein was eluted using a linear 0–500 m*M* imidazole gradient in buffer *A*. The eluted fractions (5 ml) were dialyzed against 1 l buffer *B* (50 m*M* Tris–HCl pH 8.0, 300 m*M* NaCl, 1 m*M* β-mercaptoethanol) for 16 h at 277 K. The protein was purified and the buffer exchanged for buffer *C* (50 m*M* Tris–HCl pH 8.0, 50 m*M* NaCl, 1 m*M* β-mercaptoethanol) by size-exclusion chromatography using a HR 10/30 Superdex 200 column (GE Healthcare). The purity of each of the protein samples was verified by 15% SDS–PAGE and the proteins were concentrated to 5–10 mg ml^{-1} for crystallization and *in situ* proteolysis experiments. The protein concentration was determined using a NanoDrop 2000c UV–Vis spectrophotometer (Thermo Scientific) at 280 nm using predicted extinction coefficients (calculated using *ProtParam*; http://web.expasy.org/cgi-bin/protparam/protparam; Gasteiger *et al.*, 2005) of 28 920 and 34 755 M^{-1} cm^{-1} for *Lm*SPS2 and *Tb*SPS2, respectively. The purified recombinant proteins have additional 6×His tag and thrombin-cleavage site residues, resulting in molecular weights of 44.7 and 45.0 kDa and isoelectric points of 5.83 and 5.98 for *Lm*SPS2 and *Tb*SPS2, respectively.

2.2. *In situ* proteolysis and N-terminal sequencing of *Lm*SPS2

After unsuccessful efforts to crystallize full-length *Lm*SPS2, we used an *in situ* proteolysis technique, a strategy employed to rescue proteins that are recalcitrant to crystallization (Wernimont & Edwards, 2009). The JBS Floppy-Choppy kit (Jena Bioscience) was used according to the manufacturer's instructions with the following proteases: α-chymotrypsin, trypsin, subtilisin and papain. The best result was achieved using α-chymotrypsin incubated with 5 mg ml^{-1} *Lm*SPS2 at an α-chymotrypsin:*Lm*SPS2 ratio of 1:50(*w*:*w*) for 24 h at 291 K in buffer *C* and the generated fragments were analyzed by SDS–PAGE. The α-chymotrypsin-treated *Lm*SPS2 was purified by size-exclusion chromatography (Superdex 200 10/30 HR, GE Healthcare) and transferred to a polyvinylidene fluoride membrane for N-terminal sequencing (Protein Sequence Analysis at the Department of Biochemistry, University of Cambridge). A new *Lm*SPS2 construct consisting of residues 70–398, ΔN-*Lm*SPS2, was cloned into the pET28a expression vector (Novagen) using the 5′-AGCATATGTCGGCAACGCCTGGGCAGAAG-3′ forward and 5′-AGCTCGAGTCACACCTCCACAATTTCATACCCGTC-3′ reverse primers.

2.3. Protein crystallization and data collection

For crystallization, the ΔN-*Lm*SPS2 (extinction coefficient of 27 305 M^{-1} cm^{-1} calculated using *ProtParam*; http://web.expasy.org/cgi-bin/protparam/protparam; Gasteiger *et al.*, 2005) and *Tb*SPS2 recombinant proteins were concentrated to 10 mg ml^{-1} in buffer *C*. Crystallization trials of the SPS2 proteins were set up in 96-well plates with commercial screens (Qiagen) using Honeybee (Digilab) and Crystal Phoenix (Art Robbins Instruments) robots for ΔN-*Lm*SPS2 and *Tb*SPS2, respectively. Optimization screens were carried out in 24-well plates using the hanging-drop vapour-diffusion technique with 1 µl well solution mixed with 1 µl protein solution at 10 mg ml^{-1} in buffer *C*. The microbatch experiment for *Tb*SPS2 was carried out in Greiner microbatch plates (Hampton Research) prepared with 2 µl *Tb*SPS2 at 10 mg ml^{-1} in buffer *C* mixed with 2 µl crystallization solution and 20 µl paraffin oil in each well and incubated at 291 K. The final crystallization conditions for ΔN-*Lm*SPS2 and *Tb*SPS2 were 0.2 *M* ammonium sulfate, 0.1 *M* trisodium citrate pH 5.2, 21%(*w*/*v*) PEG 4000 and 0.1 *M* trisodium citrate pH 5.6, 17%(*w*/*v*) PEG 3350, respectively. Crystals were cooled and stored in liquid nitrogen after rapid transfer to a cryoprotectant solution consisting of

their respective mother liquor with 25%(*v*/*v*) ethylene glycol for ΔN-*Lm*SPS2 crystals and 25%(*v*/*v*) MPD for *Tb*SPS2 crystals. X-ray diffraction data were collected from a single crystal at a wavelength of 0.92 Å (13 477 eV) on the I04-1 beamline at the Diamond Light Source (DLS), Harwell Science and Innovation Campus, Didcot, Oxfordshire, England (Lobley *et al.*, 2012). Integration and scaling of data were carried out using *MOSFLM* (Leslie, 2006) and *SCALA* (Winn, 2003; Evans, 2006). Data-collection and processing statistics for the crystals of ΔN-*Lm*SPS2 and *Tb*SPS2 are summarized in Table 1.

3. Results and discussion

As all attempts to crystallize *Lm*SP2 were unsuccessful, we applied *in situ* proteolysis, which has been demonstrated to be a successful approach to crystallization. This technique has demonstrated efficacy in rescuing proteins that are recalcitrant to crystallization. However, the initial crystals obtained were not suitable for X-ray diffraction experiments, probably owing to heterogeneous cleavage of the protein. Therefore, to obtain reproducible crystals we cloned the stable core of the *Lm*SPS2 protein, ΔN-*Lm*SPS2, which lacks residues 1–69, and it was obtained with high homogeneity.

N-terminal sequencing analysis of the approximately 36 kDa fragment allowed the identification of the cleavage point at the N-terminal flexible region. The resulting ΔN-*Lm*SPS2 protein yielded crystals (Fig. 1*a*) that diffracted to 1.9 Å resolution and belonged to space group $I2_12_12_1$, with unit-cell parameters a = 55.95, b = 81.69, c = 177.92 Å. Matthews coefficient calculation using the cell-content analysis program from the *CCP*4 suite is most consistent with one molecule per asymmetric unit (V_M = 2.87 Å^3 Da^{-1}, 57.21% solvent content; Winn *et al.*, 2011; Matthews, 1968).

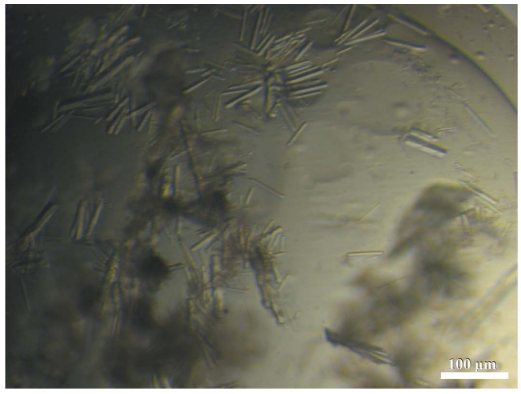

(*a*)

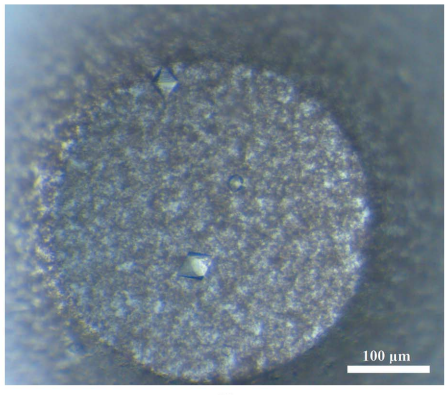

(*b*)

Figure 1
(*a*) ΔN-*Lm*SPS2 crystals observed in 0.2 *M* ammonium sulfate, 0.1 *M* trisodium citrate pH 5.2, 21%(*w*/*v*) PEG 4000 after 3 d. (*b*) *Tb*SPS2 crystals obtained after two months of incubation in 0.1 *M* trisodium citrate pH 5.6, 17%(*w*/*v*) PEG 3350 using the microbatch method (paraffin oil) in Greiner plates. These crystals were used for X-ray data collection.

Initially, the crystals obtained of *Tb*SPS2 were anisotropic with a high solvent content. Using the microbatch method, a crystal of *Tb*SPS2 grew after two months of incubation and diffracted to 3.4 Å resolution (Fig. 1*b*). The space group was $P6_422$ and the unit-cell parameters were $a = b$ = 110.69, c = 142.93 Å. The monomeric molecular weight of *Tb*SPS2 is 45 kDa and from the Matthews coefficient the crystal asymmetric unit contains one protein molecule, with a V_M of 2.94 Å^3 Da^{-1} and a solvent content of approximately 58.18%.

The first reported SPS structure from the thermophilic *A. aeolicus* was also obtained as an N-terminally truncated fragment (Matsumoto *et al.*, 2008). The selenophosphate synthetases possess a flexible N-terminal region owing to the Gly-rich loop (Itoh *et al.*, 2009). The full-length *A. aeolicus* structure shows that this loop alternates between an open and a closed conformation depending on the binding-site occupation. It is probable that the flexibility of this region allows large conformational changes, suggesting that this N-terminal loop is involved in a substrate-delivery mechanism (Itoh *et al.*, 2009). The lack of residues 1–69 of *Lm*SPS2 in ΔN-*Lm*SPS2 resulted in crystals that diffracted to a higher resolution compared with *Tb*SPS2. These results indicate that the flexibility of the N-terminal region of SPS2 interferes with protein–protein contacts during crystallization. A detailed study of the SPS N-terminal sequence is necessary to understand the importance of this region and its participation in the SPS catalytic mechanism.

The catalytic residue Sec/Cys of SPS (corresponding to Cys46 and Cys42 in *Lm*SPS2 and *Tb*SPS2, respectively) is located in the N-terminal region of *Leishmania* and *Trypanosoma* SPS2. In the ΔN-*Lm*SPS2 construct this residue is missing; however, it has been reported (Itoh *et al.*, 2009) that this conserved residue is not essential for ATP binding. This shows that although the truncated enzyme is not functional for the formation of selenophosphate, it may retain ATP hydrolysis activity.

We are now working to determine the ΔN-*Lm*SPS2 phases by the molecular-replacement methodology as implemented in *Phaser* (McCoy *et al.*, 2007) using the three-dimensional structure of human SPS1 (PDB entry 3fd5; Wang *et al.*, 2009), which shares 43% sequence identity with ΔN-*Lm*SPS2, as a search model. The structure of ΔN-*Lm*SPS2, with 66% amino-acid sequence identity, will be a good search model to solve the structure of *Tb*SPS2.

This research was supported in part by Research Grant 98/14138-2 from the Fundação de Amparo à Pesquisa no Estado de São Paulo (FAPESP). We would like to express our gratitude to Dr Victor Bolanos-Garcia for help with the N-terminal sequencing analysis and to Dr Susana A. Sculaccio for technical help during this study. We also kindly acknowledge the support received from the Department of Biochemistry of the University of Cambridge and Professor Dr Tom Blundell and the technical assistance provided to us at the N-terminal sequencing facility.

References

Aeby, E., Palioura, S., Pusnik, M., Marazzi, J., Lieberman, A., Ullu, E., Söll, D. & Schneider, A. (2009). *Proc. Natl Acad. Sci. USA*, **106**, 5088–5092.
Costa, F., Oliva, M., de Jesus, T., Schenkman, S. & Thiemann, O. (2011). *Mol. Biochem. Parasitol.* **180**, 47–50.
Donovan, J. & Copeland, P. R. (2010). *Antioxid. Redox Signal.* **12**, 881–892.
Evans, P. (2006). *Acta Cryst.* D**62**, 72–82.

Gasteiger, E., Hoogland, C., Gattiker, A., Duvaud, S., Wilkins, M. R., Appel, R. D. & Bairoch, A. (2005). *The Proteomics Protocols Handbook*, edited by J. M. Walker, pp. 571–607. Totowa: Humana Press.
Glass, R. S., Singh, W. P., Jung, W., Veres, Z., Scholz, T. D. & Stadtman, T. (1993). *Biochemistry*, **32**, 12555–12559.
Itoh, Y., Sekine, S., Matsumoto, E., Akasaka, R., Takemoto, C., Shirouzu, M. & Yokoyama, S. (2009). *J. Mol. Biol.* **385**, 1456–1469.
Leinfelder, W., Forchhammer, K., Veprek, B., Zehelein, E. & Bock, A. (1990). *Proc. Natl Acad. Sci. USA*, **87**, 543–547.
Leslie, A. G. W. (2006). *Acta Cryst.* D**62**, 48–57.
Lobley, C. M. C., Aller, P., Douangamath, A., Reddivari, Y., Bumann, M., Bird, L. E., Nettleship, J. E., Brandao-Neto, J., Owens, R. J., O'Toole, P. W. & Walsh, M. A. (2012). *Acta Cryst.* F**68**, 1427–1433.
McCoy, A. J., Grosse-Kunstleve, R. W., Adams, P. D., Winn, M. D., Storoni, L. C. & Read, R. J. (2007). *J. Appl. Cryst.* **40**, 658–674.
Matsumoto, E., Sekine, S., Akasaka, R., Otta, Y., Katsura, K., Inoue, M., Kaminishi, T., Terada, T., Shirouzu, M. & Yokoyama, S. (2008). *Acta Cryst.* F**64**, 453–458.
Matthews, B. (1968). *J. Mol. Biol.* **33**, 491–497.
Noinaj, N., Wattanasak, R., Lee, D. Y., Wally, J. L., Piszczek, G., Chock, P. B., Stadtman, T. C. & Buchanan, S. K. (2012). *J. Bacteriol.* **194**, 499–508.
Persson, B. C., Böck, A., Jäckle, H. & Vorbrüggen, G. (1997). *J. Mol. Biol.* **274**, 174–180.
Sculaccio, S., Rodrigues, E., Cordeiro, A., Magalhaes, A., Braga, A., Alberto, E. & Thiemann, O. (2008). *Mol. Biochem. Parasitol.* **162**, 165–171.
Su, D., Hohn, M. J., Palioura, S., Sherrer, R. L., Yuan, J., Söll, D. & O'Donoghue, P. (2009). *IUBMB Life*, **61**, 35–39.
Veres, Z., Kim, I. Y., Scholz, T. D. & Stadtman, T. C. (1994). *J. Biol. Chem.* **269**, 10597–10603.
Wang, K., Wang, J., Li, L. & Su, X. (2009). *J. Mol. Biol.* **390**, 747–759.
Weiss, M. S. (2001). *J. Appl. Cryst.* **34**, 130–135.
Weiss, M. S. & Hilgenfeld, R. (1997). *J. Appl. Cryst.* **30**, 203–205.
Weiss, M. S., Metzner, H. J. & Hilgenfeld, R. (1998). *FEBS Lett.* **423**, 291–296.
Wernimont, A. & Edwards, A. (2009). *PLoS One*, **4**, e5094.
Winn, M. D. (2003). *J. Synchrotron Rad.* **10**, 23–25.
Winn, M. D. *et al.* (2011). *Acta Cryst.* D**67**, 235–242.